New Visible to Broadband Shortwave Conversions for Deriving Albedos from GOES-8 Over the ARM-SGP

V. Chakrapani, D. R. Doelling, and M. M. Khaiyer
Analytical Services and Materials, Inc.
Hampton, Virginia

P. Minnis
National Aeronautics and Space Administration
Langley Research Center
Hampton, Virginia

Introduction

The radiation budget at the top of the atmosphere (TOA) is a quantity of fundamental importance to the Atmospheric Radiation Measurement (ARM) Program. Thus, it is necessary to measure the radiation budget components, broadband shortwave (SW) albedo and outgoing longwave radiation, as accurately as possible. Measurement of TOA broadband albedos over the ARM surface sites has only been possible since the advent of Clouds and the Earth's Radiant Energy System (CERES; Wielicki et al. 1998) in 1998. Prior to the availability of CERES data, it was necessary to infer the SW albedo from the visible (VIS) channel on the Geostationary Operational Environmental Satellite (GOES) imager by applying a narrowband-to-broadband (NB-BB) conversion (Minnis et al. 1995). Broadband TOA albedos have been derived from GOES-7, GOES-8, and GOES-10 data since 1994 (Khaiyer et al. 2002) as part of the National Aeronautics and Space Administration (NASA) Langley cloud and radiation products for the ARM Southern Great Plains (SGP) domain (Available at: http://www-pm.larc.nasa.gov/SGP/arm-sgp.html or at the ARM data center). The current NB-BB shortwave relationship (Minnis and Smith 1998) is based on GOES-6 VIS radiances and Earth Radiation Budget Experiment (ERBE) broadband fluxes taken during October 1986. This relationship has an uncertainty of 0.02 in the albedo, which is corresponds to a 10% root mean square (rms) error (Doelling et al. 1999), and tends to underestimate the albedo, especially for clear scenes (Rapp et al. 2002). The uncertainties in the NB-BB conversion can be eliminated by using the SW radiances measured by CERES. However, the improved spectral coverage by CERES comes at the price of reduced temporal sampling. CERES data are only available once or twice a day during 8 months of 1998, twice per day since March 2000 and four times per day since August 2002. GOES data are available every 15 or 30 minutes. To retain the temporal coverage of GOES and reduce the spectral conversion errors, it is necessary to develop an improved method for converting GOES VIS radiances to SW albedos.

In this study, CERES data are used to explore the NB-BB relationship with the ultimate goal of reducing the instantaneous uncertainties and biases in the GOES-based SW albedos. The CERES data represent an improvement over their ERBE counterparts because they have smaller footprints (10-km vs. 50-km nadir), include high-resolution cloud properties for each footprint similar to the cloud properties available in the latest NASA-Langley cloud products (Minnis et al. 2001), have improved spectral

characterization of the broadband filters, and use more robust bidirectional models (Loeb et al. 2003) to account for anisotropy of the radiance field. The CERES anisotropic corrections depend on cloud fraction, phase, optical depth τ, and 6 clear scene types, constituting nearly 600 models compared to ERBE's 12 models. The CERES SW data are correlated with the coincident NB data taken from the imagers onboard the Tropical Rainfall Measuring Mission (TRMM) and Terra satellites to develop the basis for improved NB-BB conversion functions that can be applied to GOES data taken since 1994 over the ARM SGP domain and later to other satellite data over the other ARM surface sites.

Data

The CERES Single Scanner Footprint TOA/Surface Fluxes and Clouds (SSF) product combines broadband (BB) SW (0.3-5 μm), longwave, and infrared window radiances and fluxes with imager radiances and cloud products weighted by the CERES point spread function (Geier et al. 2001). On TRMM, the CERES footprints have a nominal resolution of 10 km and the NB radiances are from the visible and infrared scanning radiometer (VIRS) imager (2-km resolution), which includes VIS (0.67 μm), 1.6-μm, 3.7-μm and two infrared window channels. The VIRS scans out to a maximum viewing zenith angle (VZA) of 47°. The TRMM data were taken from January through August 1998. TRMM is in a precessing orbit with an inclination of 35° resulting in a complete sampling of all solar zenith angles (SZAs) at a given latitude equatorward of 37°N and 37°S during its 45-day repeat cycle. The CERES instrument was in the cross track (imager) scan mode 2 out of every 3 days and in the rotating azimuth plane scan (RAPS) mode during the remaining days.

Terra is in a sun-synchronous orbit (10:30 AM local crossing time), so that for a particular latitude or region SZA is correlated with time of year. Two CERES instruments operate on Terra in the cross-track and RAPS modes simultaneously. Because only cross-track CERES data are used here, the sampling of relative azimuth angles is limited. The Terra SSF has a nominal resolution of 20 km and includes NB radiances from the moderate resolution imaging spectroradiometer (MODIS), which scans out to a VZA of ~70°. The 1-km MODIS NB radiances convolved on the SSF are from the VIS (0.64 μm) and vegetation (VEG; 0.86 μm) channels, the 1.6, 2.1, and 3.7-μm channels, and three infrared window bands. The Terra data used here were taken between November 2000 and October 2001 over the SGP domain defined by 32°N - 42°N latitudes and 105°W - 91°W longitudes.

The CERES footprints were subsetted to contain only every 3rd line and pixel. Only those footprints classified as clear (cloud fraction <5%) or overcast (cloud fraction >95%) were used in the analyses because the latest NASA-Langley cloud products classify each imager pixels (4 km nadir) as either clear or cloudy (Minnis et al. 2001).

TRMM VIS/BB Model

In the current ERBE-based NB-BB conversion, the VIS albedo is first computed from the VIS reflectance using the ERBE anisotropic directional models (ADMs) from Suttles et al. (1988). The ERBE SW albedos derived in the same manner were then correlated with the VIS albedos to develop the NB-BB conversion as a second-order function of VIS albedo with a SZA-dependent term for a land surface regardless of vegetation. The anisotropy of solar reflection, however, is dependent on scene type

and spectral band. Increasing the number of scene type and spectral ADMs and improving the accuracy of scene identification should lead to better estimated shortwave fluxes. Theoretically, BB albedo could be more accurately derived from the VIS albedo if better NB ADMs were available. One of the goals of the CERES project was to develop improved SW ADMs. Since the VIRS imager radiances on the SSF share the same viewing geometry as the CERES in cross-track mode, then, hypothetically, a VIS ADM can be built concurrently. Since the VIRS imager only scans to 47° it is not possible to build a complete VIS bidirectional model. Moreover, the cross-track scan of other imager precludes complete sampling of all parts of the limited angular space. However, a bidirectional model is not necessary, as it is possible to compute the ratio of VIS to SW BB reflectance (VIS/BB) for every angular bin sampled by VIRS and CERES. Even though the GOES VIS spectral response is broader than the VIRS VIS channel (Minnis et al. 2002), the VIRS VIS/BB model can provide insight into the development of an improved VIS/BB relationship for GOES-8.

To derive these ratios, the CERES footprints were binned with respect to the following parameters, closely following the CERES bidirectional model: five 10° VZA, nine 10° SZA, and ten relative azimuth angle bins of 20°, except for 10° in the forward and backscatter directions. Five geo-types based on the International Geosphere Biosphere Programme (IGBP) classification were defined and in order by ascending surface albedo are ocean, forest, grassland, and dark and bright desert. The VIS/BB ratios were derived for clear-sky, and ice and water clouds for each geo-type. There is sufficient sampling in most bins with the exception at high SZAs along the principal plane. Some angular bins had over 100,000 values.

The VIS/BB ratio is defined as the VIS reflectance divided by the shortwave BB reflectance and, therefore, is independent of the channel solar constants. Figure 1a shows the VIS/BB model values over clear ocean for SZA = 35°. The angular-bin means were normalized to the mean VIS/BB value given in the upper left corner of the figure using Gaussian weighting of the sampled bins. The actual VIS/BB value for each bin is the mean VIS/BB multiplied by the normalized VIS/BB as given in the colorbar. The average of the angular bin standard deviations of VIS/BB or bin uncertainty (σ) is also shown. For oceans, the VIS reflectance is greater in the forward scatter (glint) direction than the BB reflectance and less in the backscatter direction, generally following the pattern of the BB bidirectional model. This indicates that the VIS ocean reflectance is more anisotropic than the BB reflectance. On average, the VIS reflectance for grassland (Figure 1b) is 85% less than that of the BB due to the strong reflectance by green vegetation in the near infrared (NIR) spectral region (0.7-1.5 μm). The BB reflectance is also greater in the principal plane in the shadowed areas and in the "hot spot" area. Since vegetation NIR reflectance varies strongly with vegetation type and state, σ is ~20%, ranging from 0.7 to 1.0. Figure 1c shows the VIS/BB model for optically thick water clouds over grassland. For thick clouds, the spectral anisotropy from the surface should be greatly diminished. The VIS/BB model has a mean of 1.21 and is nearly uniform except for a small feature in the backscatter direction. For ice clouds (Figure 1d), the mean VIS/BB is also 1.21 and the ratio in the forward scatter direction is slightly smaller than in the backscatter direction. Both water and ice clouds have nearly the same VIS/BB value and the σ is of the order of 6%, considerably less than for clear scenes. For optically thick clouds, the VIS/BB ratio is independent of geo-type.

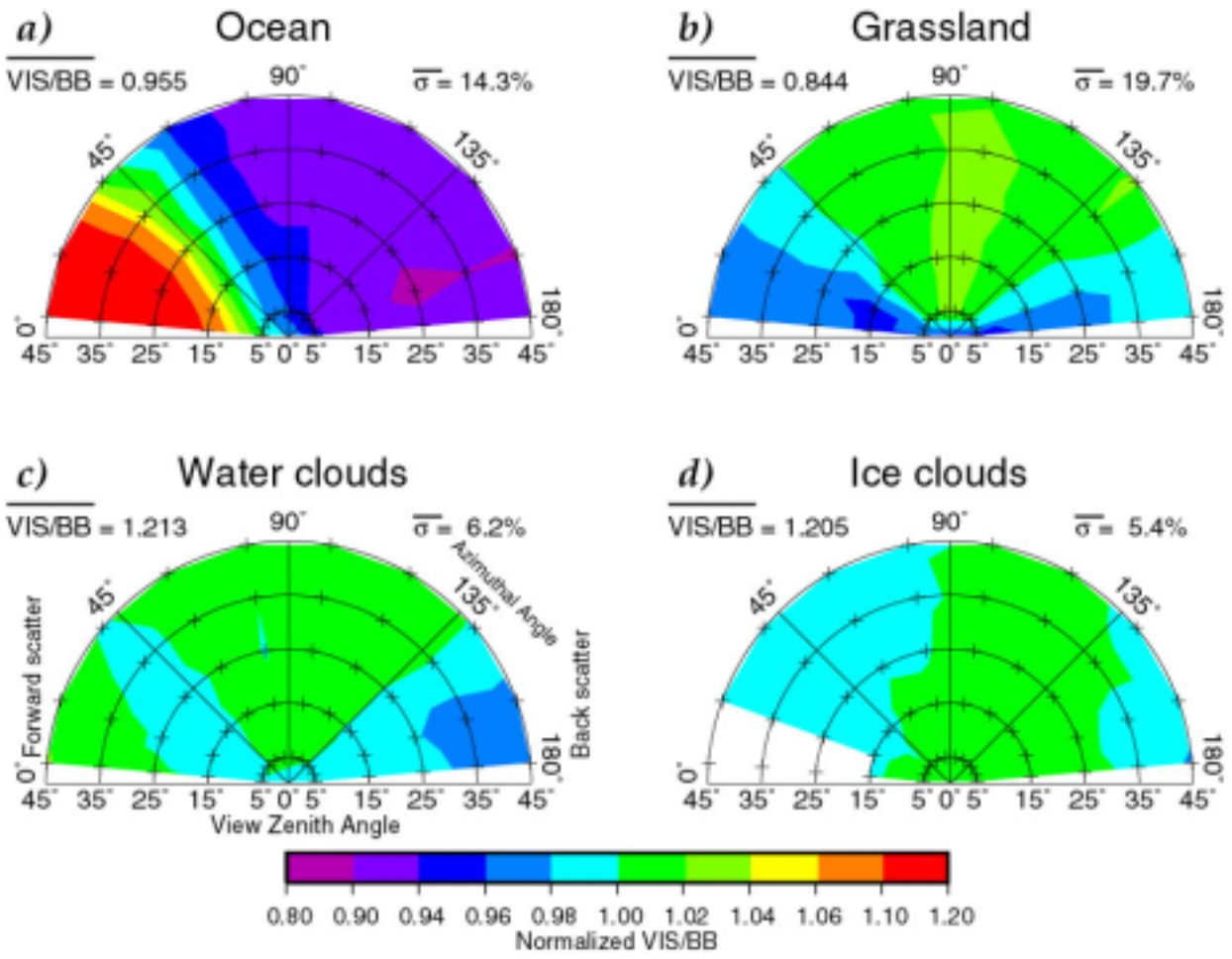

Figure 1. The TRMM VIS/BB model for a) ocean, b) grassland, c) water clouds, and d) ice clouds at a SZA of 35°. The cloud models are valid for optical depths between 18 and 40. View angle is given on the bottom of each plot and azimuth angle increases radially from left to right, where 0° is in the forward scattering direction. The mean VIS/BB for the sampled angular bins is noted on the upper left side of the plot. The average standard deviation of the bin VIS/BB in percent (σ) of the mean is given on the upper right side of the plot.

The mean VIS/BB ratios for the major categories are shown as functions of SZA in Figure 2. These values represent a partial directional VIS/BB model since the unsampled angular bins were not filled. On average, clouds are brighter in the VIS compared to the BB than any of the clear-sky geo-types because of the negligible absorption by small liquid droplets and ice crystals at wavelengths around 0.65 μm. All of the VIS/BB directional models converge toward unity near SZA = 90° due to increasing dominance of the albedo by atmospheric scattering. The smallest VIS/BB ratio for forest is at SZA = 45°. It is apparent that increasing land vegetation (decreasing surface albedo) is negatively correlated with VIS/BB and positively with σ. The range in anisotropy for clouds and deserts is about the same as the corresponding σ indicating a robust VIS/BB model. For ocean, the anisotropic range is

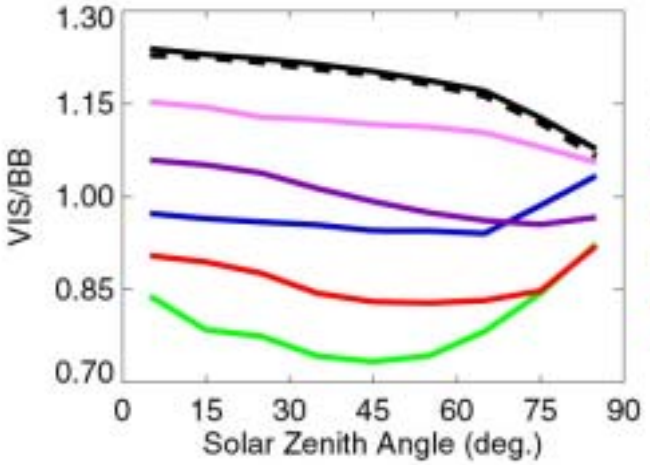

	$\overline{VIS/BB}$	σ %	Range%
Water Clouds	1.21	6.2	5.5
Ice Clouds	1.21	5.4	4.1
Bright desert	1.12	7.8	4.5
Dark desert	1.01	11.7	10.2
Ocean	0.95	14.3	30.6
Grassland	0.84	19.7	8.6
Forest	0.74	20.7	13.2

Figure 2. The partial (for sampled bins only) TRMM VIS/BB directional model with respect to SZA for the scene types given in the legend. The mean VIS/BB at a SZA of 35° is given in the left column of the table. The average standard deviation of the bin VIS/BB in percent (σ) of mean is given in the middle column. The anisotropic range in percent of mean is noted in the right column

twice that of σ. For grassland and forest, the anisotropic range is half that of the σ, indicating that the temporal and spatial variation of vegetation dominates the anisotropic signature. Thus, for land geo-types, the first order of improvement in this new NB-BB relationship, the VIS/BB ratio, would be to account for the variability of the NIR reflectance. One means for measuring the "vegetation index" using the VEG channel.

The Terra SGP Seasonal VIS/SW and VEG/VIS Cycle

Neither GOES nor VIRS has the VEG channel that is available on MODIS and the advanced very high resolution radiometer (AVHRR) on the operational NOAA sun-synchronous satellites. Although the GOES VIS channel is considerably broader than its VIRS and MODIS counterparts and includes radiation at wavelengths up to 0.8 μm, the NIR contribution is relatively minor. Thus, it is probably insufficiently sensitive to NIR radiation to track the vegetation variations and a VEG channel from another satellite is required. Operationally, the NASA-Langley GOES-derived BB fluxes could be enhanced by data from AVHRR, which is available on two or more satellites. Only clear-sky AVHRR measurements are needed and the clear-sky time periods can be determined by the GOES dataset.

The method for using the data is not immediately apparent. The spatial vegetation variability in the SGP domain, comprising crop mosaics and grasslands, is nearly as large as the seasonal cycle. The complexity of the vegetation distribution is manifest in Landsat images and land-use charts (see http://xdc.arm.gov/data_viewers/sgp_surfchar/Landsat_TM.html). Therefore, separating the SGP domain into differing vegetation types is not feasible. Determination of the VEG signal over spatial grid (0.5° by 0.5° latitude by longitude) of the operational GOES cloud products might be sufficient for accounting for the variability. Ideally, the VEG signal should be independent of the AVHRR viewing geometry, in order to correlate the VIS/BB ratio to a reference VEG albedo. Instead of computing a

VEG albedo, which needs ADMs, the simple reflectance ratio, VEG/VIS, should not be as dependent on viewing geometry. Since the VIS/BB is twice as dependent on the spatial and seasonal variation of the vegetation than the anisotropic signature, the same should hold true for VEG/VIS. To operationally estimate the VEG reflectance, the regional VEG/VIS would be multiplied by the VIS reflectance.

To determine the viewing angle dependency of VEG/VIS for clear-sky scenes, the mean VEG/VIS ratios derived from Terra MODIS data over the SGP domain were plotted in Figure 3a as functions of VZA and month to isolate the effects of SZA and vegetation seasonal cycle. As expected, the VEG/VIS ratio and VZA scatter are greatest during the summer months. No obvious VZA trend is discernable. The VEG/VIS variation with VZA for a given month is due primarily to vegetation inhomogeneities along the scan axis. VEG/VIS for all scenes with optically thick water clouds is also shown for reference. Minimal VZA and seasonal variation is evident in the cloudy plots indicating little surface contribution to the signal.

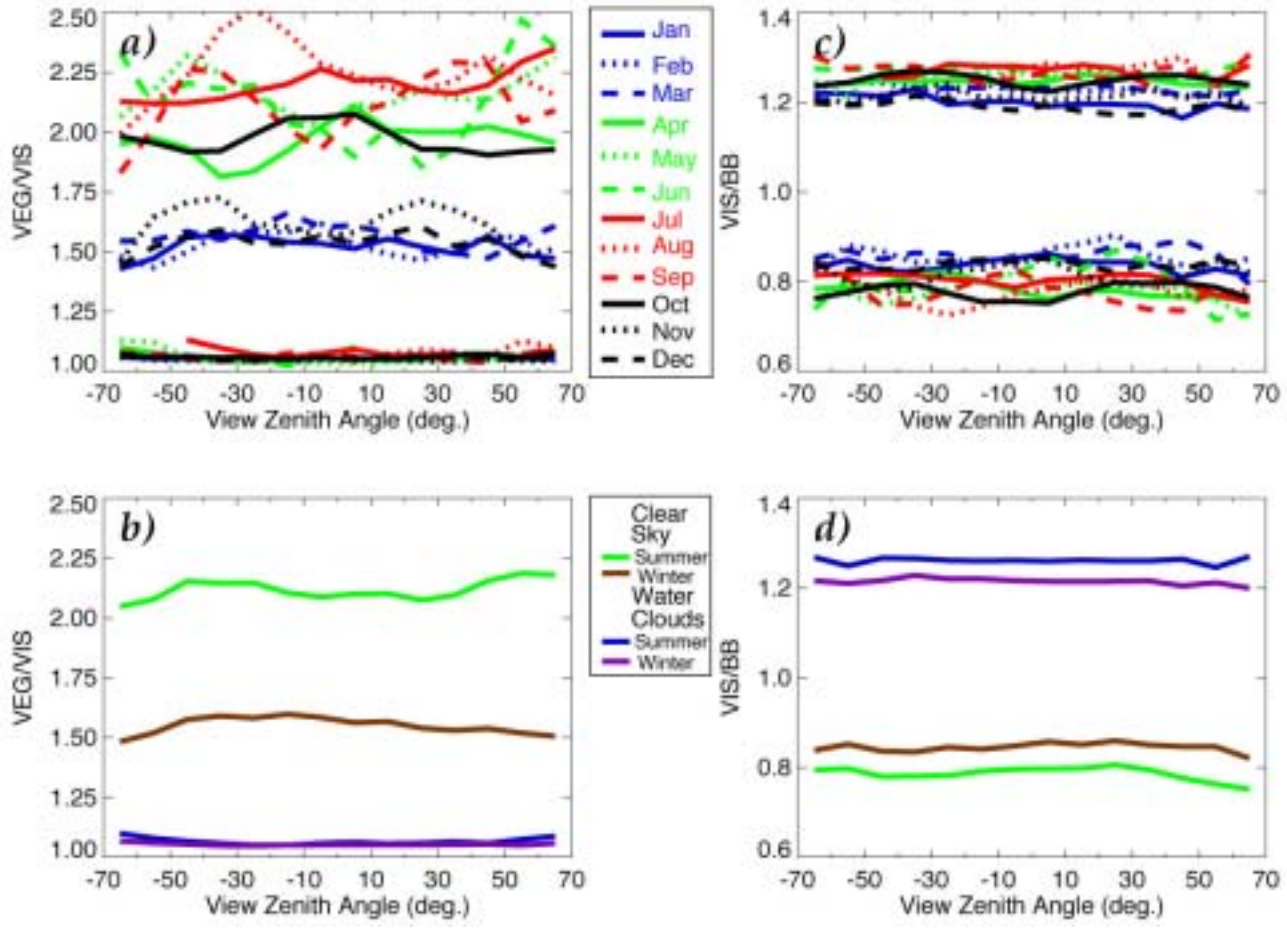

Figure 3. Monthly Terra VEG/VIS ratios over the SGP domain for clear-sky and water clouds with optical depths between 18 and 40 a) as a function of MODIS VZA, where positive angles are in the forward scatter. The summer (April-October) and winter (November-March) VEG/VIS ratios b) for clear-sky and water clouds. The corresponding VIS/BB ratios are shown in c) and d).

The bimodal seasonal cycle of vegetation is consistent with studies of vegetation phenology. Zhang et al. (2002) state that the mid-latitude vegetation annual cycle usually consists of four phases; (1) dormancy, the time period of zero physiological activity, (2) green-up, quick transition at the onset of photosynthesis, (3) maturity, the time period of maximum leaf area, and (4) senescence, rapid transition time of leaf loss and decreasing photosynthesis. Essentially the vegetation has a summer and winter phase. The summer months of April through October and the winter months of November through March were grouped together and plotted as a function of VZA in Figure 3b. The mean summer and winter VEG/VIS ratios are relatively constant with the VZA, consistent with an AVHRR analysis for Hungary during the summer (Bognar 2003). The mean monthly and seasonal variations of VIS/BB with VZA are shown in Figures 3c and 3d, respectively. Differences between the mean values of VIS/BB between summer and winter are about 0.05, a value only one tenth of that for the VEG/VIS ratios. Overall, the VZA dependence of the VEG/VIS ratio appears to be minimal and therefore it should be possible to account for the impact of the NIR on the BB radiance by including a temporal trend of VEG/VIS in the NB-BB relationship. For optically thick clouds, the VEG/VIS ratio is 1.05 whereas for VIS/BB ~1.2 indicating that clouds are slightly brighter in the VEG than in the VIS spectrum and that clouds are darker elsewhere in the spectrum. The greater separation of monthly and seasonal mean values of VIS/BB compared to those for the VEG/VIS ratios for water clouds is probably due to the dependence of the VIS/BB on SZA (Figure 2).

The Terra SGP VIS/SW and VEG/VIS Correlation with Optical Depth

The plots above show the variability in VEG/VIS and VIS/BB for clear scenes and for optically thick clouds. Real atmospheric conditions include clouds with highly variable optical depths that would have ratios different from those in Figure 3. Thus, it is necessary to account for the transition from clear skies to optically thick clouds. Optical depth is a standard variable in most cloud and radiation product datasets. It is essentially the log negative-correlation of the surface radiation contribution. A thick cloud for this study would be a cloud where τ is great enough such that VEG/VIS is constant with increasing τ. The VIS/BB ratio could still increase with optical depth but it is not associated with the VEG signal. For the Terra dataset, cloudy water and ice footprints were averaged and binned according to log τ.

Figure 4 shows VEG/VIS and VIS/BB as a function of τ. What is most striking is the difference between ice and water clouds. VEG/VIS for ice clouds monotonically tapers off exponentially to values near unity, whereas for water clouds, VEG/VIS first increases for τ <5 and then decreases exponentially. This feature is present both in summer and winter and at the monthly scale as well (not shown). Perhaps, there is multiple scattering between the surface and thin low water clouds. For the same optical depth, water clouds have a greater surface contribution because they have a lower albedo than ice clouds (Minnis et al. 1993). The variations of the VIS/BB curves have an inflection opposite to those for the VEG/VIS, including the thin water cloud feature. Again, a large VEG/VIS ratio translates to a small VIS/BB. The summer ice and winter water clouds have a similar VEG/VIS ratio for τ >3, unlike that for VIS/BB, indicating no direct relationship between VEG/VIS and VIS/BB for cloudy skies. Thick water clouds have a slightly greater SZA dependence than ice clouds, which is evident in the summer and winter VIS/BB values for τ >20.

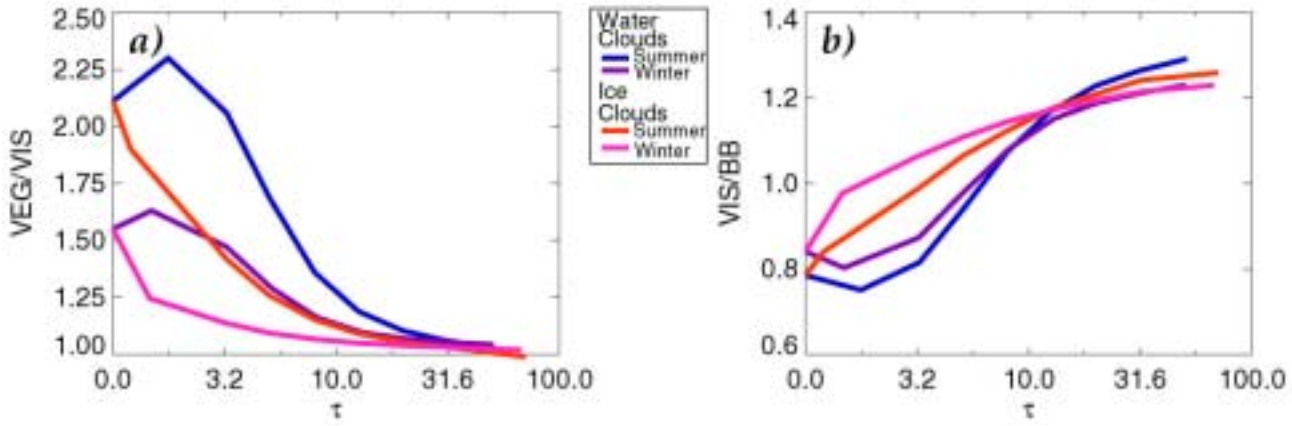

Figure 4. The Terra reflectance ratios over the SGP domain for both summer (April-October) and winter (November-March for water and ice clouds as a function of optical depth, where the clear-sky ratio is given for zero optical depth, a) VEG/VIS, b) VIS/BB.

Broadband Correlation with Multiple Spectral Channels

Most operational satellites imagers usually have a VIS and one or more other solar channels that are used in cloud property retrievals. For example, AVHRR has either a 1.6-μm and 3.7-μm channel along with the VIS and VEG channels. GOES has the VIS and 3.9-μm channels. Although the 1.6 μm and 3.7 μm radiances make up a small fraction of the BB SW radiance, they may be representative of a much larger portion of the solar spectrum and useful in estimating the TOA shortwave flux in conjunction with the VIS channel. To examine the potential for these other channels to improve the NB-BB relationship, the relevant MODIS channel radiances are regressed with the corresponding CERES SW radiances. To estimate the reflected solar portion of the 3.7-μm radiance, the emitted radiance at 3.7 μm based on the11 μm temperature using the Planck function was subtracted from the measured 3.7-μm radiance. This assumes that the temporal emissivity variations are negligible.

Table 1 shows the rms error in the estimated CERES SW radiance based on multiple and linear regressions using various combinations of MODIS spectral radiances and the CERES data for clear-sky and water and ice clouds. Clear-sky is further subdivided into summer and winter, whereas cloudy scenes are divided into two classes: all optical depths and thick clouds. The τ threshold for thick ice clouds is less than that of water clouds (Figure 4). Use of higher order terms in the regressions had negligible effect on the rms errors. The VIS radiance has the greatest single-channel correlation with SW radiance, even in summer; the squared correlation coefficient (r^2, not given in table) is 0.87. This is consistent with the earlier results; large deviations in VEG/VIS are manifest as small variations in VIS/BB. The VIS and VEG shortwave correlations are most similar in winter, (each has $r^2 = 0.91$), most likely due to the lack of any substantial reflectance by green plants, the source of most of the NIR signal in vegetation. The best dual channel correlation is the combination of the VIS and VEG channels, which reduces the rms error by 53% in summer with respect to the VIS and 38% in winter. The r^2 for VIS + VEG is 0.97. The addition of the 1.6 or 3.7 μm channels with the VIS channel reduces the rms error by less than 5% and 10% in summer and winter, respectively, and is negligible when both the VIS and VEG channels are used. For cloudy skies, the VIS channel has the lowest single-channel rms error

Table 1. RMS error ($Wm^{-2}sr^{-1}$) for regression fits based on different linear combinations of MODIS channel radiances with CERES shortwave radiance. Central wavelength given in the left column. Clear-sky results are further sub-divided into summer (April-October) and winter (November-March). Optical depth (τ) thresholds are used to sub-divide clouds into thick clouds.

MODIS Channels (μm)	Clear-Sky			Water Clouds		Ice Clouds	
	All Months	Apr-Oct	Nov-Mar	All τ	τ >18	All τ	τ >10
0.65	7.59	6.54	4.41	6.74	4.93	6.57	5.81
0.86	9.33	9.83	4.31	11.2	5.45	8.88	7.92
1.6	12.7	13.56	9.27	18.3	14.4	54.2	39.4
3.7	13.7	14.34	9.25	39.1	31.8	56.1	44.6
0.65 + 0.86	3.04	3.05	2.75	4.93	4.74	5.52	5.66
0.65 + 1.6	7.22	6.53	4.13	6.08	4.68	5.83	5.40
0.65 + 3.7	7.46	6.51	4.41	6.40	4.54	6.19	5.78
0.65 + 0.86 + 1.6	3.03	3.05	2.67	4.85	4.66	5.16	5.35
0.65 + 0.86 + 3.7	3.00	3.00	2.75	4.78	4.49	5.41	5.64
0.65 + 1.6 + 3.7	7.21	6.49	4.01	6.07	4.54	5.83	5.17

and r^2 exceeds 0.98 for all 4 categories. For thick clouds, the addition of the VEG channel to the VIS channel has an insignificant effect. For thin water and ice clouds, however, it reduces the rms error by 25% and 15%, respectively. The addition of both the 1.6-μm and 3.7-μm channels to VIS regression reduces the rms error by less than 11% in all cloud cases. There is a minimum in the reflectance for ice clouds in the 1.6-μm channel that is not the case for water clouds as a result of strong absorption by ice particles at that wavelength. This feature is evident in the 1.6-μm single-channel regression, which yields an rms error of 18.3 and 54.2 $Wm^{-2}sr^{-1}$, respectively, for water and ice clouds. In general, the contribution of each NB channel to the NB-BB relationship follows the amount of solar energy in the channel.

Conclusions

Although the MODIS and VIRS VIS spectral response is not the same as that for GOES, the results are beneficial in understanding the relationship between NB and BB radiances. The ARM-SGP NB-BB relationship for the GOES VIS channel needs to be evaluated separately for clear-sky and water and ice clouds. Up to a 50% improvement in the clear-sky relationship can be possible with the addition of VEG channel information, which can be obtained from AVHRR data. The NB-BB relationship for clouds should be formulated as a function of cloud phase, optical depth, and SZA to account for the transition clear to optically thick clouds. The VIS/BB ratio varies from 0.8 to 1.2 from clear-sky to thick clouds and could offer significant improvement in the estimation of SW fluxes from VIS radiances compared to the current method applied to ARM GOES data. The addition of the 1.6 and 3.7-μm channels can improve the relationship by up to 10%. The plan for the future GOES NB-BB relationship development will be based on coincident GOES and CERES data at the 1° level by comparing GOES VIS radiances and CERES fluxes converted to radiance using GOES-8 viewing geometry and AVHRR VEG/VIS ratios.

Acknowledgements

This research was supported by the Environmental Sciences Division of U.S. Department of Energy Interagency Agreement DE-AI02-97ER62341 and PNNL ITF No. 3407 under the ARM Program. The CERES data were obtained from the NASA Langley Research Center Atmospheric Sciences Data Center.

Corresponding Author

V. Chakrapani, v.chakrapani@larc.nasa.gov

References

Bognar, P., 2003: Correction of the effect of Sun-sensor-target geometry in NOAA AVHRR data. *Int J. Remote Sensing*, **24**, NO 10, 2153-2166.

Doelling, D. R., Smith, W. L., Jr., Minnis, P.; and Valero, F. P. J., 1999: Broadband Radiation Fluxes From Narrowband Radiances. *Proceedings of the ALPS 99 Conference*, January 18-22, 1999, Wk-P-16, 1, 5, Meribel, France.

Geier, E. B., R. N. Green, D. P. Kratz, P. Minnis, W. F. Miller, S. K. Nolan, and C. B. Franklin, 2001: Single satellite footprint TOA/surface fluxes and clouds (SSF) collection document. Available online: http://asd-www.larc.nasa.gov/ceres/ASDceres.html

Khaiyer, M. M., A. D. Rapp, P. Minnis, D. R. Doelling, W. L. Smith, Jr., L. Nguyen, M. L. Nordeen, and Q. Min, 2002: Evaluation of a 5-year cloud and radiative property dataset derived from GOES-8 data over the southern Great Plains. In *Proceedings of the Twelfth Atmospheric Radiation Measurement (ARM) Science Team Meeting*, ARM-CONF-2002. U.S. Department of Energy, Washington, D.C. Available URL: http://www.arm.gov/docs/documents/technical/conf_0204/khaiyer-mm.pdf

Loeb, N. G., N. Manalo-Smith, S. Kato, W. F. Miller, S. K. Gupta, P. Minnis, and B. A. Wielicki, 2003: Angular distribution models for top-of-atmosphere radiative flux estimation from the clouds and the earth's radiant energy system instrument on the tropical rainfall measuring mission satellite, Part. 1: Methodology. *J. Appl. Meteorol.*, **42**, 240-265.

Minnis, P., Y. Takano, and K.-N. Liou, 1993: Inference of cirrus cloud properties using satellite-observed visible and infrared radiances, Part I: Parameterization of radiance fields. *J. Atmos. Sci.*, **50**, 1279-1304.

Minnis, P., W. L. Smith, Jr., D. P. Garber, J. K. Ayers, and D. R. Doelling, 1995: "Cloud properties derived from GOES-7 for Spring 1984 ARM Intensive Observing Period using Version 1.0.0 of ARM satellite data analysis program," NASA RP 1366, p. 58.

Minnis, P., and W. L. Smith, Jr., 1998: Cloud and radiative fields derived from GOES-8 during SUCCESS and the ARM-UAV Spring 1996 Flight Series. *Geophys. Res. Lett.*, **25**, 1113-1116.

Minnis, P., W. L. Smith, Jr., D. F. Young, L. Nguyen, A. D. Rapp, P. W. Heck, S. Sun-Mack, Q. Trepte, and Y. Chen, 2001: A near-real time method for deriving cloud and radiation properties from satellites for weather and climate studies. *Proc. AMS 11th Conf. Satellite Meteorology and Oceanography*, October 15-18, pp. 477-480, Madison, Wisconsin.

Minnis, P., L. Nguyen, D. R. Doelling, D. F. Young, W. F. Miller, and D. P. Kratz, 2002: Rapid calibration of operational and research meteorological satellite imagers, Part I: Evaluation of research satellite visible channels as references. *J. Atmos. Oceanic Technol.*, **19**, 1233-1249.

Rapp, A. D., D. R. Doelling, M. M. Khaiyer, P. Minnis, W. L. Smith, Jr., and L. Nguyen, 2002: Analysis of solar absorption derived from ARM surface and satellite measurements. *Proc. 11th AMS Conf. Atmos. Rad.*, June 3-7, pp. 43-46, Ogden, Utah.

Suttles, J. T, R. N. Green, P. Minnis, G. L. Smith, W. F. Staylor, B. A. Wielicki, I. J. Walker, S. F. Young, V. R. Taylor, and L. L. Stowe, 1988: "Angular Radiation Models for Earth-Atmosphere System, Vol. 1 – Shortwave Radiation," NASA RP 1184, Vol. 1.

Wielicki, B. A., B. R. Barkstrom, B. A. Baum, T. P. Charlock, R. N. Green, D. P. Kratz, R. B. Lee, P. Minnis, G. L. Smith, D. F. Young, R. D. Cess, J. A. Coakley, D. Crommelynck, L. Donner, R. Kandel, M. D. King, A. J. Miller, V. Ramanathan, D. A. Randall, L. L. Stowe, and R. M. Welch, 1998: Clouds and the Earth's Radiant Energy System (CERES): Algorithm overview. *IEEE Trans. Geosci. Remote Sens.*, **36**, 1127-1141.

Zhang, X., M. A. Friedl, C. B. Schaaf, A. H Strahler, J. C. F. Hodges, F. Gao, B. C. Reed, and A. Huete, 2003: Monitoring vegetation phenology with MODIS. *Remote Sens. Environ.*, **84**, 471-475.